Physics Letters A 382 (2018) 1962–1967

Contents lists available at ScienceDirect

Physics Letters A

www.elsevier.com/locate/pla

Influence of liquid compressibility on the dynamics of single bubble sonoluminescence

H. Nazari-Mahroo [a], K. Pasandideh [b], H.A. Navid [a], R. Sadighi-Bonabi [b,*]

[a] Department of Laser and Optical Engineering, University of Bonab, Bonab, Iran
[b] Department of Physics, Sharif University of Technology, Tehran, Iran

ARTICLE INFO

Article history:
Received 25 February 2018
Received in revised form 27 April 2018
Accepted 28 April 2018
Available online 2 May 2018
Communicated by C.R. Doering

Keywords:
Single bubble sonoluminescence
Compressibility
Bubble collapse
Hydrochemical model

ABSTRACT

The main effects of liquid compressibility on the dynamics of single bubble sonoluminescence are investigated via three different radial dynamics models. In order to precise description of the interior gas thermodynamics, a hydrochemical model is used. In the case of an argon gas bubble in water, the results obtained with the Gilmore model and the Lezzi and Prosperetti model are compared with those resulting from the Keller and Miksis model. It is shown that the variation of liquid density at bubble surface in a very short time interval around the end of the bubble collapse, which has been incorporated into the first two models, strongly influences the bubble cavitation dynamics at higher acoustic amplitudes. The simulation results denote an increase in the bubble temperature and pressure and a reduction in the bubble minimum radius, compared with those ones obtained with Keller and Miksis model. As the acoustic amplitude increases, the difference between the models becomes larger. Moreover, it is shown that increasing the bubble ambient radius leads to an improved match between the results of the models.

1. Introduction

Single bubble sonoluminescence (SBSL), non-linear radial oscillations of a single gas bubble in liquid under the influence of a periodic acoustic wave, represents one of the challenging and interesting phenomena in physics [1–3]. The bubble expands to several times of its ambient radius and then collapses extremely quickly. The collapse is followed by afterbounces with roughly the eigenfrequency of the bubble. The main collapse of bubble is very violent and the gas within the bubble reaches extremely high temperatures, which results in promoting the chemical reactions [4]. The exchange of mass and heat between the bubble and surrounding liquid, the evaporation/condensation of water vapor molecules as well as the various chemical reactions inside the bubble at the end of collapse are very important and under investigation through many analytical and numerical models [5–9].

Although the dynamics of SBSL based on various forms of Rayleigh–Plesset (RP) equation has been extensively investigated, it is worth to mention that most of these equations use the assumption of constant liquid density at bubble surface [1,10,11]. The Keller and Miksis (KM) model is the most popular form of RP equations, which accounts for both the liquid compressibility and the radiation damping [12]. Apart from a short time interval when the bubble is close to its minimum radius, this assumption is well justified in the rest of acoustic cycle. However, it is expected that the liquid compressibility effects become more important in this short time interval [13]. Furthermore, in higher driving acoustic pressures, the speed of the bubble wall in the end of collapse approaches or surpasses the speed of sound in the liquid, contradicting the basic assumption in obtaining the RP equations, i.e. low bubble wall Mach number ($M = \dot{R}/C$) [14]. This can produce errors, though a little, in estimating the archived maximum gas temperature and pressure inside the bubble. Notably, these parameters to a large extent are responsible for the chemical reactions as well as the characteristics of the emitted light pulse from the bubble [15]. To resolve this problem, or better to say reduce its impact, the diluted forms of RP equation are usually utilized [14]. The main weakness of these approaches is diminishing the impact of compressibility on the dynamics of cavitation bubble.

Another method for resolving the mentioned problem is by considering a pressure dependent liquid density, thereby, a variable liquid sound speed, at bubble surface. In this way, both the wall Mack number is modified and the liquid compressibility is modeled more accurately [16]. This possibility correctly has been incorporated in the original Gilmore (G) model [17] and also in the Lezzi and Prosperetti (LP) model [18]. The main advantage of these models is the accounting for a pressure dependent liquid density

* Corresponding author.
E-mail address: sadighi@sharif.ir (R. Sadighi-Bonabi).

https://doi.org/10.1016/j.physleta.2018.04.058
0375-9601/

at bubble surface, which exhibits the liquid compressibility effect on the dynamics of cavitation bubble more completely [19].

The differences between the predictions of mentioned models on the extent of the liquid compressibility impact have already been explored [16,20–23]. However, these comparative studies have been made based on the simplified models for interior gas thermodynamics. As far as we know, no complete comparative study based on the hydrochemical model for interior gas thermodynamics has already been reported. Fuster et al. [21] compared the results obtained by solving the partial differential equations governing conservation of mass, momentum, and energy with those attained by other mentioned radial dynamic models and validated the accuracy of these models in higher acoustic amplitudes. However, the effective processes such as mass transfer and chemical reactions were not included in the calculations. It is worth mentioning that at higher acoustic amplitudes, the mass and heat transfer from the bubble wall are particularly important [13]. Zilonova et al. [23] investigated the bubble dynamics in viscoelastic soft tissue in high-intensity focal ultrasound thermal therapy by using some cavitation models. They showed that viscoelastic models coupled with Gilmore model produce more reliable results than the other cavitation models. However, this study was conducted in soft tissue medium and the chemical reactions were neglected in the simulation.

In this study, to gain a more in-depth insight into the effects of liquid compressibility on the dynamics of SBSL at higher driving pressures, the G and LP models are used for exploring the radial oscillations of bubble. The interior gas thermodynamics is described by a hydrochemical model in which the mass and heat transfer, as well as the chemical reactions, are included. Moreover, the results are compared with those obtained with KM model. The investigation of the extent of liquid density variation in collapse stage and its impact on the dynamics of SBSL are the main objectives of the present study.

2. Summary of the models

One of the most popular and widely used models for description the radial dynamics of the bubble in sonoluminescence literature is Keller and Miksis model [12].

$$\left(1-\frac{\dot{R}}{C_0}\right)R\ddot{R}+\frac{3}{2}\left(1-\frac{\dot{R}}{3C_0}\right)\dot{R}^2 = \left(1+\frac{\dot{R}}{C_0}+\frac{R}{C_0}\frac{d}{dt}\right)\left[P_l-P_{ac}(t)-P_0\right] \tag{1}$$

Here dots denote time derivatives, R is the bubble radius, C_0 and ρ_0 are the ambient liquid sound speed and density, P_l is the liquid pressure at bubble surface, P_0 is the ambient pressure, and P_{ac} is the driving acoustic pressure. The acoustic pressure is $P_{ac}=-P_a\sin(2\pi ft)$; P_a is the amplitude and f its frequency.

For further including the effect of liquid compressibility in collapse stage of bubble, Lezzi and Prosperetti developed a model based on the enthalpy of the host liquid [18]:

$$\left(1-\frac{\dot{R}}{C_0}\right)R\ddot{R}+\frac{3}{2}\left(1-\frac{\dot{R}}{3C_0}\right)\dot{R}^2 = \left(1+\frac{\dot{R}}{C_0}+\frac{R}{C_0}\frac{d}{dt}\right)\left[H_l-\frac{1}{\rho_0}P_{ac}\left(t+\frac{R}{C_0}\right)\right] \tag{2}$$

Here H_l is the difference between the liquid enthalpy at the bubble wall and at infinity:

$$H_l=\int_{P_0}^{P_l}\frac{dp}{\rho_l} \tag{3}$$

This integral is calculated by using the modified Tait's equation [24]:

$$\frac{P+B}{P_\infty+B}=\left(\frac{\rho_l}{\rho_\infty}\right)^n \tag{4}$$

where $B=3049.13$ atm and $n=7.15$ are valid for water up to 10^5 bars. Also ρ_l is the liquid density at bubble surface, which in this model is not considered as constant. This equation also allows for variable sound speed at the surface of bubble.

$$C_l=\sqrt{C_0^2+(n-1)H_l} \tag{5}$$

It is obvious that for the case in which $C_l=C_0$, $H_l=(P_l-P_0)/\rho_0$, and $\rho_l=\rho_0$, the Eq. (2) reduces to Eq. (1).

It is worth to note that Eq. (2) is a form of a most general Gilmore (G) model [17], in which the variation of liquid density is only considered in calculating the integral in Eq. (3). The Gilmore model reads as:

$$\left(1-\frac{\dot{R}}{C_l}\right)R\ddot{R}+\frac{3}{2}\left(1-\frac{\dot{R}}{3C_l}\right)\dot{R}^2 = \left(1+\frac{\dot{R}}{C_l}\right)H_l+\left(1-\frac{\dot{R}}{C_l}\right)\frac{R}{\rho_l C_l}\frac{dH_l}{dt} \tag{6}$$

It is noticed that in the Gilmore model the lower limit of integral in Eq. (3) is P_a+P_0, instead of P_0 in LP model. The Eqs. (1), (2) and (6) must be supplemented by an expression relating the pressures inside and outside the bubble interface. An explicit expression for this linking equation can be obtained from the normal stress balance at the bubble interface [12]:

$$P_l=P_g-\frac{4\mu\dot{R}}{R}-\frac{2\sigma}{R} \tag{7}$$

Here, μ is the shear viscosity of the host liquid and σ is the surface tension coefficient. The gas pressure inside the bubble P_g is given by the van der Waals equation of state [25]:

$$P_g=\frac{N_{tot}k_BT_g}{V-N_{tot}B} \tag{8}$$

where k_B is the Boltzmann's constant, N_{tot} is the total number of particles within the bubble, V is the volume of bubble, and T_g is the gas temperature. The hard-core parameter $B=5.1\times10^{-29}$ m^3 is assumed equal for all particles.

The total rate of change in the particles number is due to the mass diffusion and chemical reactions. For an argon bubble in water, a kinetic mechanism consisting in eight elementary chemical reactions, involving the chemical species O_2, OH, H, O, H_2O and H_2 is used. The kinetic mechanism used in the present study was detailed in the [25,26]. Here, only a summary of the fundamental equations of the model is presented below.

In this chemical model the general form for the reaction rates of a chemical process $M+A+B\leftrightarrow M+C+D$, by using modified Arrhenius laws, is expressed as

$$r_{f,j}=\left[\frac{\exp[n_{tot}B/(1-n_{tot}B)]}{1-n_{tot}B}\right]^j k_{f,j}n_{tot}n_An_BT^{c_{f,j}}\exp\left(-\frac{E_{f,j}}{kT}\right)$$
$$r_{b,j}=k_{b,j}n_{tot}n_Cn_DT^{c_{b,j}}\exp\left(-\frac{E_{b,j}}{kT}\right) \tag{9}$$

Here, $n_{A,\ldots,D}$ is the concentration of the species, n_{tot} is the total number density of the species, and r_j is the net reaction rate per unit volume given by the difference between the forward and backward rates $r_{f,j}$ and $r_{b,j}$. Also, $k_{f,j}$ and $k_{b,j}$ are the frequency

Table 1
The considered chemical reactions and the values of Arrhenius parameters. The activation energies $E_{f,j}/k$ and $E_{b,j}/k$ are given in K and the reaction energies ΔE_j are in kJ/mol.

No.	Reaction	t_j	$k_{f,j}$	$c_{f,j}$	$\frac{E_{f,j}}{k}$	$k_{b,j}$	$c_{b,j}$	$\frac{E_{b,j}}{k}$	ΔE_j
1	$O + O + M \leftrightarrow O_2 + M$	1	1.2×10^{17}	−1	0	3.16×10^{19}	−1.3	59893	498
2	$O + H + M \leftrightarrow OH + M$	1	5×10^{17}	−1	0	3.54×10^{17}	−0.9	51217	428
3	$O + H_2 \leftrightarrow OH + H$	0	3.87×10^{4}	2.7	3150	1.79×10^{4}	2.7	2200	−8
4	$H + O_2 \leftrightarrow O + OH$	0	2.65×10^{16}	−0.7	8576	9×10^{13}	−0.3	−83	−70
5	$H + H + M \leftrightarrow H_2 + M$	1	10^{18}	−1	0	7.46×10^{17}	−0.8	52177	436
6	$H + OH + M \leftrightarrow H_2O + M$	1	2.2×10^{22}	−2	0	3.67×10^{23}	−2	59980	498
7	$OH + H_2 \leftrightarrow H + H_2O$	0	2.16×10^{8}	1.5	1726	5.2×10^{9}	1.3	9529	62
8	$OH + OH \leftrightarrow O + H_2O$	0	3.57×10^{4}	2.4	1062	1.74×10^{6}	2.2	7693	70

factors which are given in $cm^3\,(mol/s)$ for the two-body reactions and in $cm^3\,(mol^2/s)$ for the three-body reactions. Table 1 shows the considered chemical reactions and the values of Arrhenius parameters for argon bubble in water.

The chemical rate of change of species i is calculated by the sum over all elementary reaction rates with their corresponding stoichiometric weight $\alpha_{i,j}$.

$$\dot{N}_i^c = V \sum_j \alpha_{i,j} r_j \tag{10}$$

The rate of change of the particle number due to mass diffusion is calculated by means of boundary layer approach [25,27]:

$$\dot{N}_i^d = 4\pi R^2 D \frac{n_i}{l_d}, \qquad l_d = \min\left(\sqrt{\frac{RD}{|\dot{R}|}}, \frac{R}{\pi}\right) \tag{11}$$

where n_i is the instantaneous concentration of particle species i. The coefficient D is the diffusion coefficient given by $D = D_0(n_0/n_{tot})$, where $D_0 = 23.55 \times 10^{-6}$ m^2/s, n_{tot} is the instantaneous total number density of the bubble and n_0 is the value of n_{tot} at the beginning of the bubble evolution. The quantity l_d is the thickness of the diffusive boundary layer.

Time evolution of the gas temperature is calculated from the energy equation of the bubble content [25,28]:

$$\begin{aligned}
&\dot{T}_g \sum_i \frac{\partial e_{th,i}}{\partial T_g} N_i = \dot{Q} - P_g \dot{V} - \sum_i e_{th,i} \dot{N}_i + \dot{E}_{chem} + \sum_i h_{w,i} \dot{N}_i^d \\
&h_{w,i} = \left(1 + \frac{f_i}{2}\right) k_B T_B \\
&e_{th,i} = \frac{f_i}{2} k_B T_B + \sum_l \frac{k_B \Theta_{i,l}}{e^{\Theta_{i,l}/T_g} - 1}
\end{aligned} \tag{12}$$

Here $\dot{E}_{chem}$ denotes the rate of change in the chemical energy of the bubble due to chemical reactions, $e_{th,i}$ is the thermal energy of the molecule with $\Theta_{i,l}$ as the various characteristic vibrational temperatures of the particle. The quantity $h_{w,i}$ is the molecular enthalpy of particle i at the bubble wall temperature T_0, and f_i is the sum of its translational and rotational degrees of freedom. Also $\dot{Q}$ is the rate of heat transfer between the bubble and the liquid, which is defined by the method developed in [25]:

$$\dot{Q} = 4\pi R^2 \kappa \frac{T_0 - T_g}{l_{th}}, \qquad l_{th} = \min\left(\sqrt{\frac{R\chi}{|\dot{R}|}}, \frac{R}{\pi}\right) \tag{13}$$

Here, κ, l_{th}, and χ are the thermal conductivity coefficient of the gas inside the bubble, the thickness of the thermal boundary layer, and the thermal diffusivity coefficient of the bubble content, respectively.

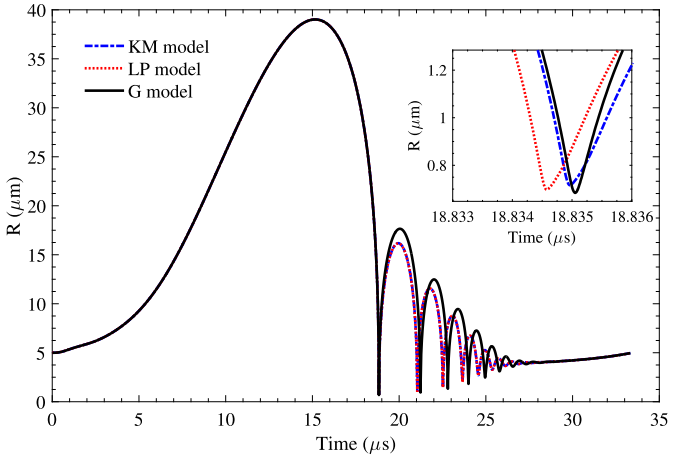

Fig. 1. The variation of the bubble radius during one acoustic cycle, computed with G model (solid), LP model (dotted), and KM model (dash-dotted). Inset: the magnified part of bubble radius evolution around the end of collapse.

3. Results and discussion

Fig. 1 shows the time evolution of bubble radius as calculated with the three compared models in this study under the typical parameter's values of argon bubble in water; $R_0 = 5$ μm, $P_0 = 1.0$ atm, $P_a = 1.3$ atm, $f = 30$ kHz, $\sigma = 0.07$ $N\,m^{-1}$, $\mu = 0.001$ Pa s, $T_0 = 20\,^{\circ}C$, and $\rho = 998$ $kg\,m^{-3}$. The values of other chemical and physical parameters of the system are taken from [28].

This figure reveals that in the expansion stage, there is no distinguishable difference between the results of three considered models. However, in the collapse stage, where the liquid compressibility becomes important, a significant difference appears. The minimum radius of bubble computed with the G, LP, and KM models are 0.684 μm, 0.697 μm, and 0.716 μm, respectively (see the inset in Fig. 1). As a direct result, the compression ratio (R_{max}/R_{min}) in the Gilmore model is higher than LP and KM models. With the used conditions, the simulations reveal the same trend for the maximum gas temperature reached at the end of the collapse, the lower the bubble minimum radius, the higher the gas maximum temperature. The maximum gas temperature computed with the Gilmore model is 18906 K, while this value decreases to 16154 K and 13470 K when using the LP model and the KM model, respectively. This result matches the previous finding of Fuster et al. [21], where the effect of liquid compressibility was investigated by a complete PDE model and the results were compared with those obtained using the KM and Gilmore models. The values of gas temperature and pressure with the complete model were higher than the ones calculated with the mentioned models. Also, the KM and Gilmore models presented the similar predictions regarding the cavitation bubble characteristics. However, in our present study, the values of maximum temperature and pressure inside the bubble obtained by models with pressure depen-

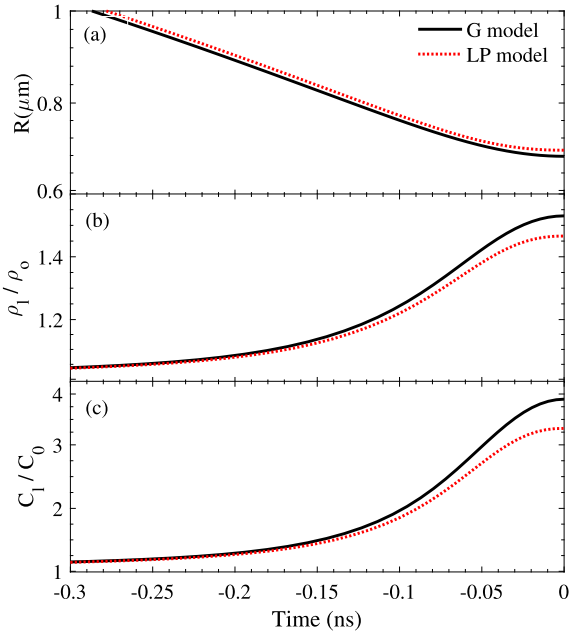

Fig. 2. The time evolution of (a) the bubble radius, (b) the liquid density, and (c) the liquid sound speed just before the end of the collapse, retrieved with the G and LP models for the same parameters and constants as in Fig. 1. Zero time corresponds to the moment of minimum bubble radius.

dent liquid density (the Gilmore and LP models) are higher than those computed by KM model in which the liquid density on bubble surface remains constant. This finding reveals that considering the mass and heat diffusion between the bubble and surrounding liquid and the chemical reactions leads to pushing the results of the LP and Gilmore models towards the predictions of complete model at higher driving pressures.

Furthermore, the KM and LP models predict the same behavior for bubble radius evolution in afterbounces stage, while the Gilmore model predicts a higher value for the amplitude of bubble oscillations in this stage, as was previously reported in [22,29].

The differences between the three compared models in this study arise from the liquid density variation included in the Gilmore and LP models. In the expansion stage, where the wall motion is slow, the liquid density on bubble surface remains constant. Nevertheless, the change in liquid density is expected in a short time interval around the end of collapse, when the bubble approaches its minimum radius. For instance, Fig. 2 shows the time development of the bubble radius, the liquid density, and the liquid sound speed in a short time just before the end of collapse as retrieved by these models. From Fig. 2(b) and 2(c), a considerable increase in the values of the liquid density and liquid sound speed is observed. The time duration of these polemical variations is less than one nanosecond. In this short time fraction of bubble oscillation cycle, the liquid pressure on the bubble surface increases dramatically; consequently, a thin liquid layer around the bubble is highly compressed as the local speed of sound increases. Accordingly, the wall Mach number, at least to some extent, is modified and the reliability of the approach is further improved. It is noticed that this modification is also observed in the bubble bounces but with lower intensity, due to the softer collapses in afterbounces stage.

Compared to LP model, the liquid is compressed more intensely in G model. This is due to the fact that the G model includes more details of the liquid compressibility [13].

At the final moments of bubble collapse, the dynamics of bubble motion is far more rapid than the diffusion dynamics of water vapor. Therefore, not all the water vapor molecules escape during compression. The entrapped water molecules are subjected to extremely high temperature and pressure reached during bubble collapse and undergo fast dissociation to produce various radicals. Fig. 3 illustrates the variation of the number of various chemical species at around the end of collapse as returned by the LP model at acoustic amplitude of 1.2 atm. The values of other parameters are the same as in Fig. 1. It can be seen that the peak of H molecules is higher than the other chemical species. Also, the damping rate of the number of this molecule is considerably higher than the other chemical products. It is worth mentioning that for the condition used ($P_a = 1.2$ atm), the pressure and temperature inside the bubble calculated with the three compared models are very close together. Therefore, no significant difference in the amount of chemical products simulated by the considered models is expected. However, as mentioned before, the main purpose of the present study is on the effects of liquid compressibility on the dynamical characteristics of SBSL and the chemical reactions inside the bubble are not explored.

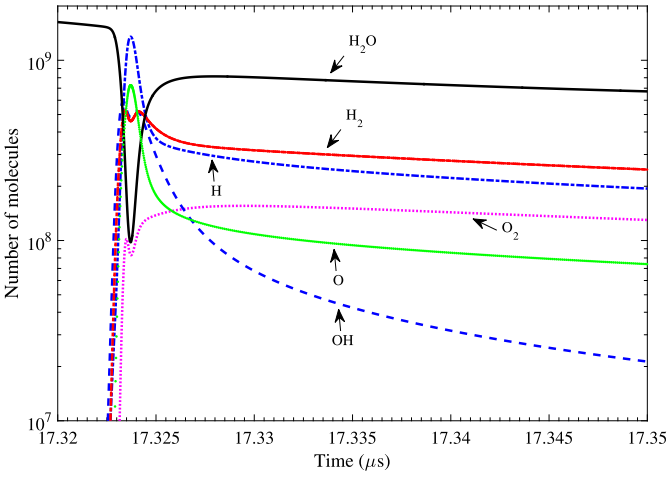

Fig. 3. The evolution of the various reaction products inside the bubble at around the end of bubble collapse according to LP model for $P_a = 1.2$ atm. The values of other parameters are the same as in Fig. 1. The vertical axis is in logarithmic scale.

To capture the major effects of the liquid compressibility on the bubble dynamics, simulations were performed under the various acoustic amplitudes up to 1.3 atm. The obtained results are summarized in Table 2. In order to have a better comparison between the values of maximum wall velocity attained by three considered models, the wall Mach number is defined as the maximum wall velocity divided by the ambient liquid sound speed.

From Table 2, it can be concluded that the Gilmore model predicts a lower minimum radius and higher maximum gas temperature compared to KM and LP models. The greater the acoustic amplitude is, the higher the noticed difference is. For instance, when taking the values attained with the KM model as reference, the relative difference in maximum gas temperature between the KM and LP model equals 11% at acoustic amplitude of 1.22 atm. This value reaches 18% when increasing the acoustic amplitude to 1.28 atm, while the difference between the KM and Gilmore models reaches 32%. Furthermore, the difference between the LP and Gilmore models grows with acoustic amplitude. For example, even these two models give the same value for the maximum gas temperature at 1.22 atm; however, the simulation result shows a 13% difference between them at 1.28 atm, when taking the values of LP model as reference. These findings reveal that the liquid compressibility taken into account in the LP and Gilmore models changes the bubble cavitation dynamics at higher acoustic amplitudes.

In Fig. 4, the variation of the maximum gas temperature and the maximum wall Mach number as function of bubble ambient radius are compared for the three considered models at acoustic

Table 2
Summary of the bubble collapse characteristics for a 5 μm bubble driven under various acoustic amplitudes, retrieved by three considered models.

P_a (atm)	Model	R_{max} (μm)	R_{min} (μm)	Compression ratio	V_{max}/C_0	T_{max} (10^3 K)
1.2	KM	29.29	0.783	37.41	−0.421	9.18
	LP	29.29	0.763	38.36	−0.432	9.99
	G	29.29	0.768	38.13	−0.417	9.76
1.22	KM	31.24	0.758	41.20	−0.513	10.29
	LP	31.24	0.739	42.28	−0.526	11.44
	G	31.24	0.738	42.34	−0.551	11.49
1.24	KM	33.19	0.742	44.74	−0.605	11.25
	LP	33.19	0.723	45.91	−0.621	12.75
	G	33.19	0.717	46.26	−0.607	13.28
1.26	KM	35.14	0.730	48.09	−0.696	12.08
	LP	35.14	0.712	49.35	−0.714	13.94
	G	35.14	0.703	49.98	−0.702	15.10
1.28	KM	37.08	0.722	51.33	−0.786	12.81
	LP	37.08	0.704	52.68	−0.805	15.07
	G	37.08	0.692	53.55	−0.797	16.97
1.3	KM	39.01	0.716	54.47	−0.872	13.47
	LP	39.01	0.697	55.93	−0.893	16.15
	G	39.01	0.684	57.02	−0.890	18.91

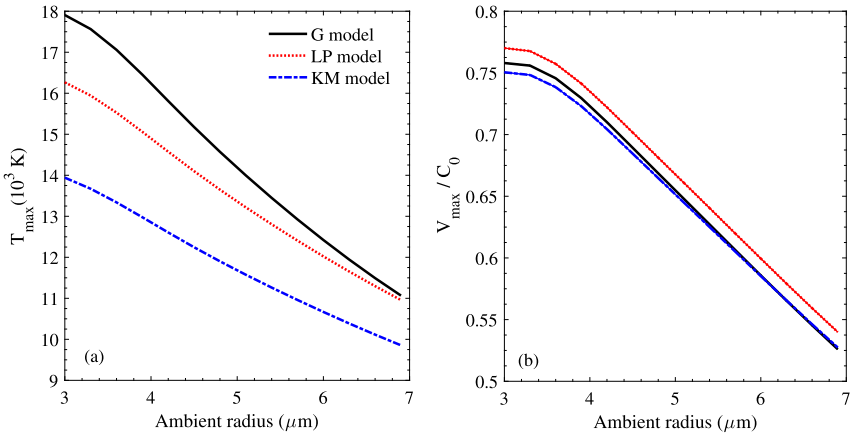

Fig. 4. The variation of (a) the maximum gas temperature and (b) the wall Mach number with respect to bubble ambient radius at $P_a = 1.25$ atm, obtained with the Gilmore (solid), the LP (dotted), and KM (dash-dotted) models.

amplitude of 1.25 atm. From Fig. 4(a), it can be seen that the maximum gas temperature decreases by increasing bubble ambient radius. Meanwhile, the consistency between the models is improved. Notably, the Gilmore and LP models give a close estimation for the gas temperature inside the bubble at large bubble ambient radius. This is a direct consequence of the reduction of the collapse strength with increasing the bubble ambient radius. The same trend encountered for the wall velocity when increasing the bubble ambient radius, as shown in Fig. 4(b).

4. Conclusion

The effects of liquid compressibility on the dynamics of single bubble sonoluminescence at higher driving pressures are explored via Gilmore model and Lezzi and Prosperetti model (with a pressure dependent liquid density at the bubble surface) as well as Keller and Miksis model (with constant liquid density). In order to have a more accurate comparison between the models, a hydrochemical model for precise description of the interior gas thermodynamics is utilized. In the case of argon bubble in water, the simulation results denote that including liquid density variation leads to a considerable modification of bubble cavitation dynamics during the collapse stage. The wall Mach number and the minimum radius of bubble decrease. Also, the pressure and temperature inside the bubble increase. The difference between the results obtained with the two categories of models increases in higher acoustic amplitudes. Moreover, it is shown that increasing the bubble ambient radius leads to a better match between the results of the compared models in this study. These observations indicate that according to the operational parameters, especially under high acoustic amplitudes, the thermal and dynamical characteristic of the cavitation bubble are somewhat sensitive to the selected radial model. The models that allow for pressure dependent liquid density at bubble surface produce a more reliable result compared to the model with constant liquid density, due to including the compressibility of liquid around in a more complete way.

References

[1] W. Lauterborn, T. Kurz, Physics of bubble oscillations, Rep. Prog. Phys. 73 (2010) 106501, https://doi.org/10.1088/0034-4885/73/10/106501.
[2] P.-K. Choi, K. Takumori, H.-B. Lee, Na emission and bubble instability in single-bubble sonoluminescence, Ultrason. Sonochem. 38 (2017) 154–160, https://doi.org/10.1016/j.ultsonch.2017.03.015.
[3] M. Gheshlaghi, R. Sadighi-Bonabi, A. Ghadirifar, The effect of KZK pressure equation on the sonoluminescence in water and fat tissues, Phys. Lett. A 379 (2015) 1951–1959, https://doi.org/10.1016/j.physleta.2015.06.045.

[4] S. Merouani, O. Hamdaoui, Y. Rezgui, M. Guemini, Theoretical estimation of the temperature and pressure within collapsing acoustical bubbles, Ultrason. Sonochem. 21 (2014) 53–59, https://doi.org/10.1016/j.ultsonch.2013.05.008.
[5] K.S. Suslick, D.J. Flannigan, Inside a collapsing bubble: sonoluminescence and the conditions during cavitation, Annu. Rev. Phys. Chem. 59 (2008) 659–683, https://doi.org/10.1146/annurev.physchem.59.032607.093739.
[6] J. Liang, W. Chen, X. Wang, J. Yang, Z. Chen, Evidence of mass exchange between inside and outside of sonoluminescing bubble in aqueous solution of terbium chloride, Phys. Lett. A 380 (2016) 4105–4108, https://doi.org/10.1016/j.physleta.2016.10.031.
[7] K. Kerboua, O. Hamdaoui, Computational study of state equation effect on single acoustic cavitation bubble's phenomenon, Ultrason. Sonochem. 38 (2017) 174–188, https://doi.org/10.1016/j.ultsonch.2017.03.005.
[8] A. Moshaii, R. Rezaei-Nasirabad, K. Imani, M. Silatani, R. Sadighi-Bonabi, Role of thermal conduction in single-bubble cavitation, Phys. Lett. A 372 (2008) 1283–1287, https://doi.org/10.1016/j.physleta.2007.09.014.
[9] J. Liang, W. Chen, C. Zhou, W. Cui, Z. Chen, Line emissions from sonoluminescence in aqueous solutions of halide salts without noble gases, Phys. Lett. A 379 (2015) 497–500, https://doi.org/10.1016/j.physleta.2014.11.051.
[10] A. Prosperetti, A. Lezzi, Bubble dynamics in a compressible liquid. Part 1. First-order theory, J. Fluid Mech. 168 (1986) 457–478, https://doi.org/10.1017/S0022112086000460.
[11] R. Sadighi-Bonabi, F.A.F. Lahiji, F. Razeghi, The effect of viscosity, applied frequency and driven pressure on the laser induced bubble luminescence in water–sulfuric acid mixtures, Phys. Lett. A 380 (2016) 2219–2226, https://doi.org/10.1016/j.physleta.2016.02.050.
[12] J.B. Keller, M. Miksis, Bubble oscillations of large amplitude, J. Acoust. Soc. Am. 68 (1980) 628–633, https://doi.org/10.1121/1.384720.
[13] C. Cogné, S. Laboureт, R. Peczalski, O. Louisnard, F. Baillon, F. Espitalier, Theoretical model of ice nucleation induced by acoustic cavitation. Part 1: pressure and temperature profiles around a single bubble, Ultrason. Sonochem. 29 (2016) 447–454, https://doi.org/10.1016/j.ultsonch.2015.05.038.
[14] M.P. Brenner, S. Hilgenfeldt, D. Lohse, Single-bubble sonoluminescence, Rev. Mod. Phys. 74 (2002) 425–484, https://doi.org/10.1103/RevModPhys.74.425.
[15] K. Kerboua, O. Hamdaoui, Influence of reactions heats on variation of radius, temperature, pressure and chemical species amounts within a single acoustic cavitation bubble, Ultrason. Sonochem. 41 (2018) 449–457, https://doi.org/10.1016/j.ultsonch.2017.10.001.
[16] L. Yuan, H.Y. Cheng, M.-C. Chu, P.T. Leung, Physical parameters affecting sonoluminescence: a self-consistent hydrodynamic study, Phys. Rev. A 57 (1998) 4265–4280, https://doi.org/10.1103/PhysRevE.57.4265.
[17] F.R. Gilmore, The Growth or Collapse of a Spherical Bubble in a Viscous Compressible Liquid, Hydrodynamics Laboratory, California Institute of Technology, Pasadena, California, USA, 1952, Report No. 26-4.
[18] A. Lezzi, A. Prosperetti, Bubble dynamics in a compressible liquid. Part 2. Second-order theory, J. Fluid Mech. 185 (1987) 289–321, https://doi.org/10.1017/S0022112087003185.
[19] W. Lauterborn, R. Mettin, Acoustic cavitation: bubble dynamics in high-power ultrasonic fields, Power Ultrason. (2015) 37–78, https://doi.org/10.1016/B978-1-78242-028-6.00003-X.
[20] A. Prosperetti, Y. Hao, Modelling of spherical gas bubble oscillations and sonoluminescence, Philos. Trans. R. Soc., Math. Phys. Eng. Sci. 357 (1999) 203–223, https://doi.org/10.1098/rsta.1999.0324.
[21] D. Fuster, C. Dopazo, G. Hauke, Liquid compressibility effects during the collapse of a single cavitating bubble, J. Acoust. Soc. Am. 129 (2011) 122–131, https://doi.org/10.1121/1.3502464.
[22] G. Chen, Y. Lu, Cavitation in compressible supercritical carbon dioxide, Phys. Chem. Liq. 53 (2015) 67–74, https://doi.org/10.1080/00319104.2014.915711.
[23] E. Zilonova, M. Solovchuk, T.W.H. Sheu, Bubble dynamics in viscoelastic soft tissue in high-intensity focal ultrasound thermal therapy, Ultrason. Sonochem. 40 (2018) 900–911, https://doi.org/10.1016/j.ultsonch.2017.08.017.
[24] F.A. Godínez, M. Navarrete, Influence of liquid density on the parametric shape instability of sonoluminescence bubbles in water and sulfuric acid, Phys. Rev. A 84 (2011) 16312, https://doi.org/10.1103/PhysRevE.84.016312.
[25] X. Lu, A. Prosperetti, R. Toegel, D. Lohse, Harmonic enhancement of single-bubble sonoluminescence, Phys. Rev. A 67 (2003) 56310, https://doi.org/10.1103/PhysRevE.67.056310.
[26] A. Moshaii, K. Imani, M. Silatani, Sonoluminescence radiation from different concentrations of sulfuric acid, Phys. Rev. A 80 (2009) 46325, https://doi.org/10.1103/PhysRevE.80.046325.
[27] R. Toegel, B. Gompf, R. Pecha, D. Lohse, Does water vapor prevent upscaling sonoluminescence?, Phys. Rev. Lett. 85 (2000) 3165–3168, https://doi.org/10.1103/PhysRevLett.85.3165.
[28] K. Imani, F. Bemani, M. Silatani, R. Sadighi-Bonabi, Ambient temperature effect on single-bubble sonoluminescence in different concentrations of sulfuric acid solutions, Phys. Rev. A 85 (2012) 16329, https://doi.org/10.1103/PhysRevE.85.016329.
[29] S. Hilgenfeldt, M.P. Brenner, S. Grossmann, D. Lohse, Analysis of Rayleigh–Plesset dynamics for sonoluminescing bubbles, J. Fluid Mech. 365 (1998) 171–204, https://doi.org/10.1017/S0022112098001207.